Journal of Zhejiang University SCIENCE A
ISSN 1673-565X (Print); ISSN 1862-1775 (Online)
www.zju.edu.cn/jzus; www.springerlink.com
E-mail: jzus@zju.edu.cn

Machining distortion prediction of aerospace monolithic components*

Yun-bo BI†1, Qun-lin CHENG[2], Hui-yue DONG[1], Ying-lin KE[1]

([1]*State Key Lab of Fluid Power Transmission and Control, Zhejiang University, Hangzhou 310027, China*)

([2]*Shanghai Spaceflight Precision Machinery Research Institute, Shanghai 201600, China*)

†E-mail: zjubyb@zju.edu.cn

Received May 23, 2008; Revision accepted Dec. 5, 2008; Crosschecked Mar. 4, 2009

Abstract: To predict the distortion of aerospace monolithic components, a model is established to simulate the numerical control (NC) milling process using 3D finite element method (FEM). In this model, the cutting layer is simplified firstly. Then, the models of cutting force and cutting temperature are established to gain the cutting loads, which are applied to the mesh model of the part. Finally, a prototype of machining simulation environment is developed to simulate the milling process of a spar. Key factors influencing the distortion, such as initial residual stress, cutting loads, fixture layout, cutting sequence, and tool path are considered all together. The total distortion of the spar is predicted and an experiment is conducted to validate the numerical results. It is found that the maximum discrepancy between the simulation results and experiment values is 19.0%

Key words: Monolithic component, Machining distortion, Finite element simulation
doi:10.1631/jzus.A0820392 **Document code:** A **CLC number:** TG5

INTRODUCTION

With the increasing demands of superior component performance, quality control of a machined part is becoming critical, especially in the manufacturing process of thin-walled large size aerospace monolithic components. During the last decade, many researches have been done to predict the part deformation due to material processing by using finite element method (FEM). Tsai *et al*.(1999), Ratchev *et al*.(2003) and Wan *et al*.(2005) studied the static form errors in peripheral milling of thin-walled low-rigidity workpieces, but these works only focused on the localized static elastic deformation induced during milling operation, and only considered the impact of cutting force. Recently, the total distortion problem has received a lot of attention. Wang and Padmanaban (2004), Åström (2004) and Wang *et al*.(2005) simulated the machining distortion of thin-walled part caused by redistribution of residual stress during the material removal process, and concluded that the residual stress is one of the main causes of machining distortion. Dong *et al*.(2003) studied the workpiece distortion induced by the residual stress under different clamping conditions, and concluded that clamping points have a great effect on the residual stress distribution that affects machining distortion. Under a given initial residual stress and clamping condition, Guo *et al*.(2005) studied the effect of tool-path on the machining distortion of thin-walled frame part. Furthermore, by considering the effects of residual stress, fixture layout and cutting force, Mei *et al*.(2005) simulated the machining distortion of aerocraft arc-shaped workpiece. Despite a significant amount of research in this area, still there is lack of a comprehensive model to predict machining distortion by taking into account the effects of residual stress, cutting loads, fixture layout, cutting sequence, and tool path.

Spar, as one of the principal aerospace monolithic components, is widely used in aircraft structures. In this study, the practical milling process of spar is

* Project (No. 50435020) supported by the National Natural Science Foundation of China

considered as a coupled thermo-mechanical process, and the machining distortion is studied based on the analysis step modeling method. The work does not focus on the localized static elastic deflection, but the total distortion. Key factors influencing distortion such as initial residual stress, cutting loads, fixture layout, cutting sequence, and tool path are considered all together to reveal the machining distortion. To validate the modeling method, a milling process of a spar is simulated, and the numerical results of machining distortion are compared with the experimental results.

SIMPLIFICATION OF CUTTING LAYER

In the milling process, the cutting edge travels on a trochoidal path due to the feeding rate and the spindle rotation, and the undeformed chip is formed, as shown in Fig.1a. To build up an efficient finite element (FE) model, hexahedral elements are used. Since the hexahedral elements can hardly match the real shape of undeformed chip, it is necessary to simplify its shape. Simplification must conform to two principles: one is that the simplified mesh is convenient for removing materials and applying loads, and the other is the calculation efficiency can be improved distinctly. Therefore, a simplified cutting layer model is adopted to mesh the workpiece, as shown in Fig.1b. v_f is the feed speed, a_p is the axial cutting depth, a_e is the radial cutting depth and d_w is the thickness of cutting layer. d_w is equal to the width of the transient cutting surface in feed direction, which is calculated as follows (Liu *et al*., 2006):

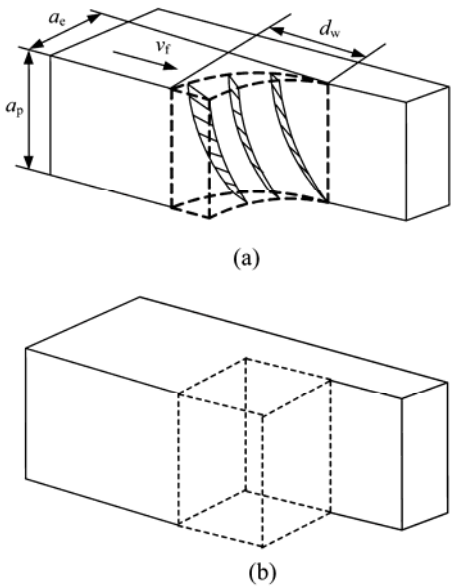

Fig.1 (a) Actual cutting layer; (b) Simplified cutting layer

$$d_w = \sqrt{R^2 - (R - a_e)^2}, \quad (1)$$

where R is the radius of cutting tool.

CUTTING FORCE AND CUTTING TEMPERATURE MODEL

Cutting force modeling

As shown in Fig.2, an FE model is used to gain the cutting force, which was verified in (Cheng *et al*., 2006). The flat end mill with two flutes has a diameter of 10 mm, a helix angle of 32°, a rake angle of 20° and a clearance angle of 15°. The workpiece material is aluminum alloy 7050-T7451. The cutting force simulation avoids calibration of cutting force coefficients. The cutter is regarded as a rigid body, and the workpiece is modeled as a thermo-elastic-plastic material model. Under the conditions of a given friction coefficient, heat conduction coefficient between tool and chip, and material property, a commercial software package Deform-3D is used to conduct the cutting force simulation. During the simulation, the cutter rotates around the negative Z direction at a given spindle rotation speed and moves along the negative X direction at a given feeding rate.

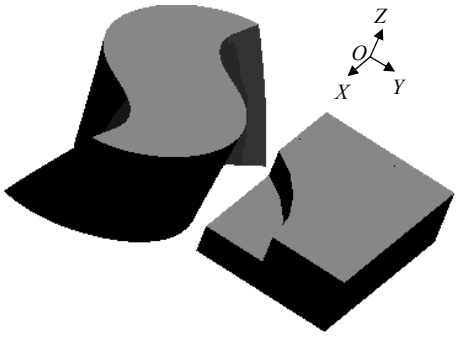

Fig.2 Finite element model of cutting force simulation

Cutting temperature modeling

To simulate the temperature field, the heat conduction analysis has been implemented based on the principle of solid heat conduction. The quantity of

heat flowing into the workpiece needs to be calculated. The heat produced by the primary shear zone, the secondary shear zone and the tertiary zone in metal cutting has different contribution to the temperature distribution. The heat produced by the primary shear zone plays the principal role in the temperature field distribution (Altintas, 2000). The heat produced by the secondary shear zone mainly influences the temperature of chip and cutter. Although the friction between the machined surface and tool clearance face also generates heat, the quantity of heat flowing into the workpiece is small enough to be ignored (Oxley, 1989). As shown in Fig.3, the heat source in milling is simplified to a band heat source. Due to the shear deformation of the primary shear zone in the cutting process, the band heat source is generated at every cutting time. The tool cutting edge cuts into at Point 1 and out at Point 2. During the whole cutting process, the band heat source $L_hL'_h$ can be regarded as a continuous moving band heat source. Then, it is a procedure of heat diffusion until the next tool cutting edge cuts in at Point 1. When the next tool cutting edge cuts in, a new band heat source is generated again until the tool cutting edge cuts out. So, the heat source during the milling process is regarded as a periodic discontinuous band heat source. For the heat analysis of workpiece, the discontinuous milling process is equivalent to a procedure where the moving band heat source heats the workpiece periodically.

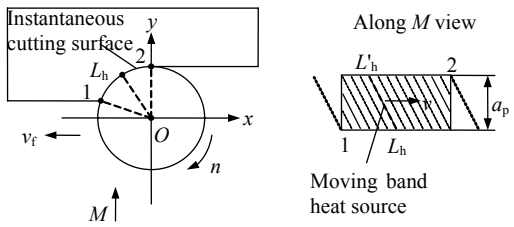

(a) (b)

Fig.3 Illustration of band heat source. (a) Along *z* direction; (b) Along *M* direction

The shear energy (U_{sh}) produced by the shear force in the primary shear zone is expressed as

$$U_{sh}=F_{sh}v_{sh}, \tag{2}$$

where F_{sh} is the shear force acting on the shear plane, and v_{sh} is the shear velocity.

The shear force acting on the shear plane is expressed as

$$F_{sh}=\left\{(-F_x\cos i+F_y\sin i)^2+(-F_x\sin i\cos\phi_n-F_y\cos i\cos\phi_n-F_z\sin\gamma_n)^2\right\}^{1/2}, \tag{3}$$

where F_x, F_y and F_z are the cutting forces achieved by simulation; i is the cutting edge inclination angle and equal to the helix angle of the cutter; γ_n is the normal rake angle; ϕ_n is the normal shear angle and can be obtained by finite element simulation of the orthogonal metal cutting process.

The shear velocity is expressed as

$$v_{sh}=\frac{\cos\gamma_e}{\cos(\phi_e-\gamma_e)}v, \tag{4}$$

where v is the cutting velocity, γ_e is the effective rake angle and determined by Eq.(5), and ϕ_e is the effective shear angle and determined by Eq.(6):

$$\gamma_e=\arcsin(\sin\gamma_n\cos^2 i+\sin^2 i), \tag{5}$$

$$\phi_e=\arcsin\left(\frac{\cos\eta_{sh}\cos\gamma_e}{\cos i\cos\gamma_n}\sin\phi_n\right), \tag{6}$$

where η_{sh} is the chip flow angle measured in the shear plane, defined as (Shaw, 1984):

$$\tan\eta_{sh}=\frac{\tan i\cos(\phi_n-\gamma_n)-\tan i\sin\phi_n}{\cos\gamma_n}. \tag{7}$$

It is assumed that the shear energy is transformed to heat completely. Part of the heat is removed by the chip, and the rest flows into the workpiece. The intensity Q of the band heat source flowing into the workpiece is defined as

$$Q=R_wF_{sh}v_{sh}, \tag{8}$$

where R_w is the ratio of the heat flowing into the workpiece and can be obtained as (Loewen and Shaw, 1954)

$$R_w=1-R_l=1-\left(1+1.328\left(\alpha\gamma_{sh}/(va_p)\right)^{1/2}\right)^{-1}=\left(1+0.753\left(va_p/(\alpha\gamma_{sh})\right)^{1/2}\right)^{-1}, \tag{9}$$

where R_1 is the ratio of the heat flowing into the chip, α is the coefficient of thermal diffusivity, and γ_{sh} is the shear strain defined as

$$\gamma_{sh}=\cot\phi_n+\tan(\phi_n-\gamma_n). \quad (10)$$

Application of cutting loads

In this study, a method is adopted to apply the cutting loads to the corresponding mesh nodes shown in Fig.4. Firstly, the cutting force is obtained by means of FE simulation. Then, the cutting force is discretized in time domain. Finally, every discrete cutting force is applied evenly to the relevant nodes according to the time sequence. Through Eq.(8), the intensity of the band heat source can be calculated at any time during the cutting period. By applying band heat source varying with the time to the relevant nodes, the temperature field distribution of workpiece is simulated. As the cutting process goes on, the heat source will be applied to different cutting positions. The characteristic of cutting force and heat source fluctuated dynamically with time is described as a time-load function curve in FE solver.

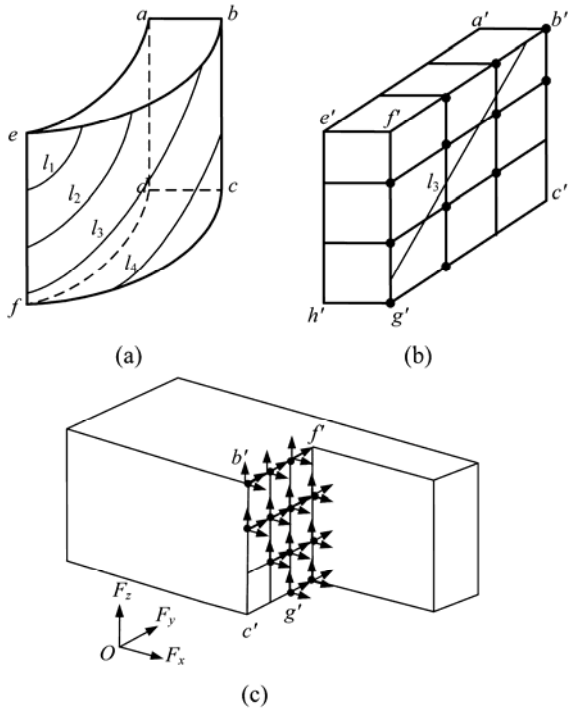

Fig.4 Application of cutting load. (a) Helical line load; (b) Simplified straight line load; (c) Equivalent point load. The dot represents the mesh nodes that the line load l_3 acts on

In Fig.4a, l_1, l_2, l_3 and l_4 represent the helical line loads acting on the chip by the cutting edge of cutting tool at four different time points. After simplification of cutting layer, the helical line load can be simplified as a straight line load shown in Fig.4b. After the hexahedral mesh of the simplified cutting layer is generated, the line load can be equivalent to a point load acting on the mesh nodes. The cutting loads are applied on these mesh nodes uniformly.

MILLING PROCESS MODELING AND SIMULATION OF AEROSPACE MONOLITHIC COMPONENTS

Geometric model

The geometric model of a spar with pockets is shown in Fig.5. The workpiece material is aluminum alloy 7050-T7451. The axial and radial cutting depths are both 3 mm, the feeding rate is 1430 mm/min, and the rotation speed is 1.1×10^4 r/min. The thicknesses of thin-wall and thin-web are both 2 mm.

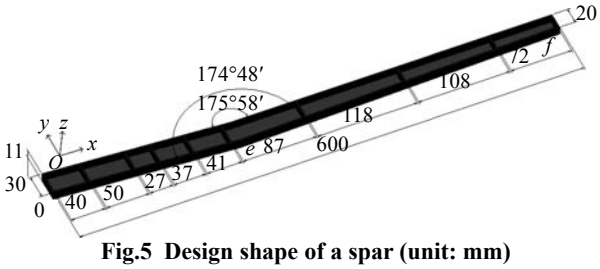

Fig.5 Design shape of a spar (unit: mm)

Application of initial residual stress

The initial residual stress exists in the blank due to previous material fabrication and heat treatment processes before machining, which is one of the key factors to induce the part distortion. The equilibrium equation met by initial residual stress is expressed as

$$\int\sigma_r dA=0, \text{ and } \int dM=0, \quad (11)$$

where σ_r is the initial residual stress existing in the pre-stretched blank, A is the area of cross section, and M is the moment produced by the initial residual stress.

The workpiece material is gradually removed in milling, and the rigidity of workpiece is changed. Due to the releasing of residual stress, the initial equilibrium state of residual stress is broken, and the deformation must be generated to establish a new

equilibrium state.

The initial blank geometry shape is shown in Fig.6. As shown in Fig.7, the initial residual stress inside the blank is measured by a layer-removed method, and the initial stress value in each layer is supposed to be constant. The initial residual stress is applied to FE model layer-by-layer. That is to say, the residual stress curve is discretized evenly into N stress values satisfying Eq.(11), where N is equal to the layer number of finite element meshes along thickness direction, and the stress values are applied to corresponding layer of meshes using specific routine supported by FE solver.

Fig.6 Blank geometry of a spar

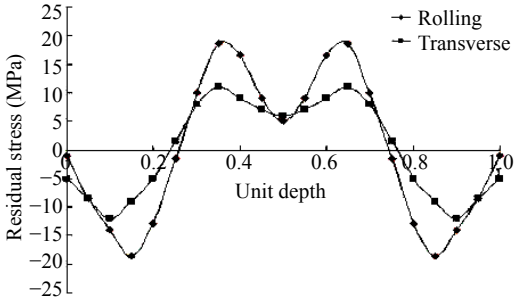

Fig.7 Initial residual stress inside the blank of a spar

Cutting sequence and tool path

The cutting sequence of pockets in a spar is from left to right in turn. The tool path of each pocket is from inner to outer shown in Fig.8, which is widely used in workshop. The tool path is generated in the commercial software package Unigraphics/CAM.

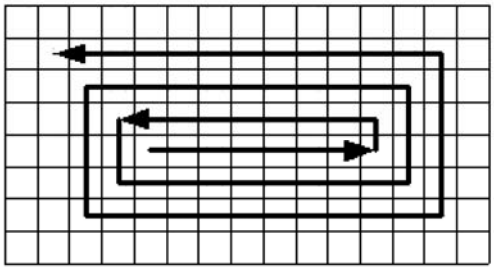

Fig.8 Cutting path of milling process simulation

Finite element simulation of milling process

A prototype of simulation environment is developed in C++ to control the whole milling processes including generating finite element mesh, applying boundary condition and fixture constraint, cutting loads, removing mesh elements, mapping field data, importing, and parsing tool path, etc. (Bi, 2007). The commercial FE solver ABAUS/Standard is used as the default solver.

During the simulation, the finite element mesh should be generated appropriately to meet the analysis requirement. Because there are 9 pockets in the spar, each pocket is considered as a simulation unit. In the mesh model, the uncut region is meshed more sparsely, and the mesh is regenerated once after a pocket is finished. The first and the second pockets of the spar are meshed shown in Fig.9a and Fig.9b, respectively. The other pockets can be meshed according to the same method.

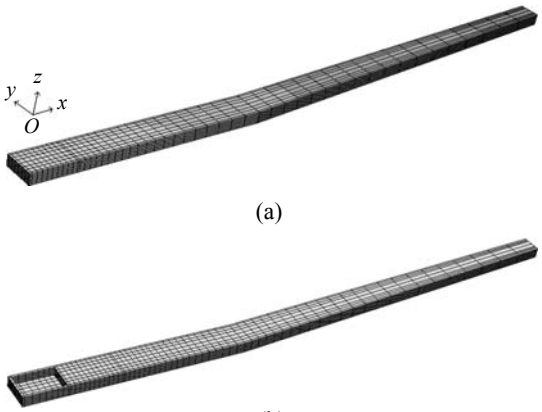

(a)

(b)

Fig.9 Mesh model of a spar for (a) milling pocket 1 and (b) milling pocket 2

The milling process simulation is divided into two phases to carry out by using the coupled thermo-mechanical module of FE solver: one is a milling process simulation with fixture, and the other is a free distortion simulation of part without fixture after milling. In the first phase, key factors, such as initial residual stress, cutting loads and fixture have important effects on the part distortion, and will change the stress distribution state in the workpiece. The large quantity of distortion energy has been generated and congregated in the workpiece. In the second phase, the distortion energy releases without fixture, then the inner stress redistributes, and the part

distorts freely. The basic procedure of process simulation in the first phase can be described as follows: each analysis step is composed of two substeps, one is the simulation with cutting loads during the cutting period, and the other is the simulation without cutting loads during the uncut period. The fixture condition is converted into the constraint boundary condition. Because the workpiece is placed on the worktable of machine tool, the x, y, z degrees of freedom (DOFs) of the workpiece bottom surface are constrained. Because the thin-walls of workpiece are clamped in the practical milling process, the outer surfaces of thin-walls are also constrained. In the second phase, the free distortion simulation of part can be described as follows: firstly, unload all constraints in the first simulation phase, then select three noncollinear points on the workpiece bottom surface to constrain their x, y, z DOFs, y, z DOFs and z DOF, respectively. The so-called 3-2-1 constraints are used to ensure the free distortion of the part, and to avoid its rigid motion caused by stress redistribution.

During simulation, the initial workpiece temperature is set to room temperature (20 °C). Because heat exchange exists between the bottom of workpiece and worktable of machine tool, the bottom surface of workpiece is defined as heat exchange surface. The heat generated during cutting enters the environment through the front, back, left and right surfaces of workpiece, so these surfaces are also defined as the exchange surfaces.

SIMULATION RESULTS

The stress and temperature distributions of a spar at some time during simulation are shown in Figs.10a and 10b. The highest temperature and the biggest stress occur in the local cutting region, which is the same as that in the metal cutting mechanism simulation. The total distortions of a spar are shown in Fig.11. Bend distortions protruding towards machined surface are produced, and the maximum distortion location of a spar lies in 251 mm.

The angle change of the middle corner of a spar is shown in Fig.12. The angle value of the spar has an increase of 0.09°. Due to the bend distortion and the change of corner angle, the torsion also happens at the small end of part.

EXPERIMENTS VERIFICATION

To verify the FE simulation, a practical machining experiment was performed with the parameters in Geometric model subsection. The machine tool is FIDIA HS 664 RT (FIDIA corporation, Italy). The cutting sequence and tool path are also generated

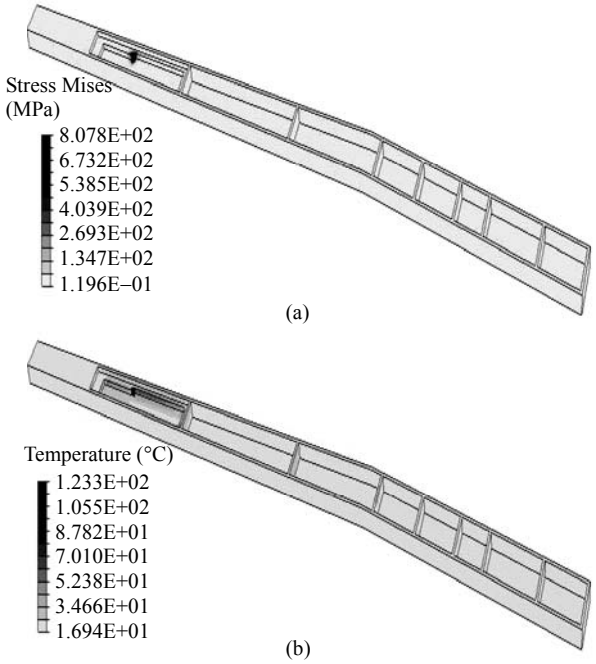

Fig.10 (a) Stress distribution and (b) temperature distribution of a spar at some time

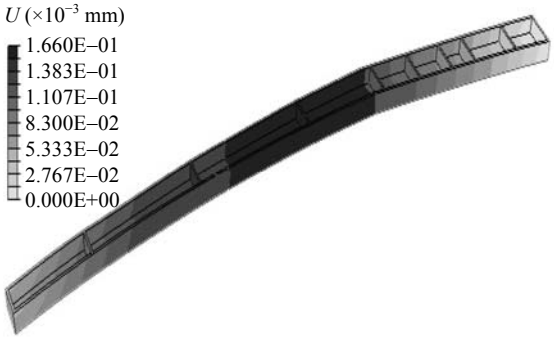

Fig.11 Total distortion of a spar

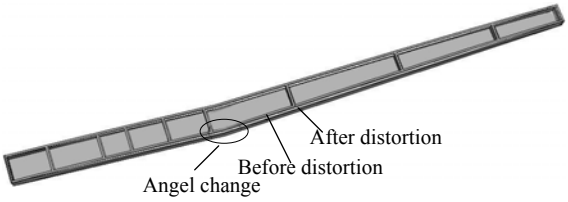

Fig.12 Angle change of a spar

by the commercial software package Unigraphics/ CAM, which is the same as the simulations. The photo of machining experiment is shown in Fig.13. Fig.14 shows the machined spar.

Fig.13 Experimental photo

Fig.14 Machined part

To display the part distortion, the plug guage is laid on the spar's deformation area, as shown in Fig.14, which shows clearly that the distortion tendency is a bend distortion protruding towards machined surface. To express the distortion accurately, one edge *oef* shown in Fig.5 is chosen to measure the distortion value, and *o* is the origin of coordinate. The experiment and simulation results are shown in Fig.15, and the maximum distortion values are 0.205 mm and 0.166 mm, respectively, and the maximum discrepancy between the simulation and experiment is 19.0%, which shows that the experiment result agrees well with the simulation. The maximum distortion location of the spar lies in 248 mm. The corner angle around the middle of the spar is also measured, and its value has an increase of 0.124°. The change tendencies of corner angles also agree well with the simulation. Due to the bend distortion and the change of corner angle, the torsion is also produced at the small end of part.

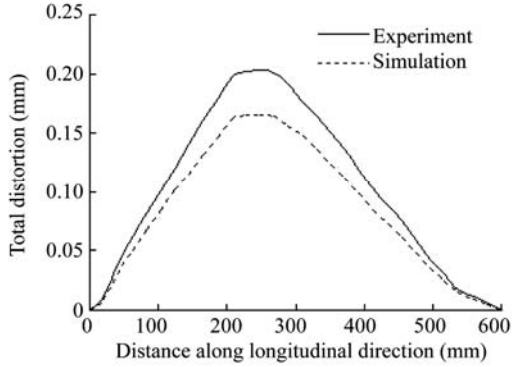

Fig.15 Distortion comparison of the spar

CONCLUSION

A physics-based material processing simulation model is proposed to predict machining distortion of aerospace monolithic component in this study. Some key factors, such as initial residual stress, cutting loads, fixture, cutting sequence and tool path are introduced synthetically into the FE model of a milling process.

The milling process of a spar is simulated based on the established FE model, and the distortion is achieved successfully. The distortion tendency consists of bend and torsion. The milling experiment is carried out under the same cutting condition as that in the simulation, and the distortion of bend and torsion is also produced and measured. For distortion, the maximum discrepancy between the simulation and experiment is 19.0%. It shows that the modeling presented is valid and can be used to predict the machining distortion.

References

Altintas, Y., 2000. Manufacturing Automation. Cambridge University Press, Cambridge, England, p.4-13.

Åström, P., 2004. Simulation of Manufacturing Processes in Product Development. PhD Thesis, Luleå University of Technology, Sweden.

Bi, Y.B., 2007. Physics-based Milling Process Simulation and Applications in Machining Distortion Prediction of Aeronautical Monolithic Components. PhD Thesis, Zhejiang University, Hangzhou, China (in Chinese).

Cheng, Q.L., Ke, Y.L., Dong, H.Y., 2006. Numerical simulation study on milling force for aerospace aluminum alloy. *Acta Aeronautica et Astronautica Sinica*, **27**(4):724-727 (in Chinese).

Dong, H.Y., Ke, Y.L., Wu, Q., Xu, D., 2003. Finite element model for optimal clamping scheme of frame shape workpiece based on residual stress distribution. *Acta Aeronautica et Astronautica Sinica*, **24**(4):382-384 (in Chinese).

Guo, H., Zuo, D.W., Wang, S.H., Xu, L.L., Wang, M., 2005. Effect of tool-path on milling accuracy under clamping. *Transactions of Nanjing University of Aeronautics & Astronautics*, **22**(3):234-239.

Liu, S.G., Zheng, L., Zhang, Z.H., Wen, D.H., 2006. Optimal fixture design in peripheral milling of thin-walled workpiece. *International Journal of Advanced Manufacturing Technology*, **28**(7-8):653-658. [doi:10.1007/s00170-004-2425-8]

Loewen, E.G., Shaw, M.C., 1954. On the analysis of cutting tool temperatures. *ASME Journal of Engineering for Industry*, **76**:217-231.

Mei, Z.Y., Wang, Y.Q., Fan, Y.Q., 2005. Researching and

simulating deformation of aerocraft structure part in NC machining. *Acta Aeronautica et Astronautica Sinica*, **26**(2):234-239 (in Chinese).

Oxley, P.L.B., 1989. Mechanics of Machining, an Analytical Approach to Assessing Machinability. Ellis Horwood Limited, West Sussex, England.

Ratchev, S., Govender, E., Nikov, S., Phuah, K., Tsiklos, G., 2003. Force and deflection modelling in milling of low-rigidity complex parts. *Journal of Materials Processing Technology*, **143-144**(12):796-801. [doi:10.1016/S0924-0136(03)00382-0]

Shaw, M.C., 1984. Metal Cutting Principles. Clarendon Press, Oxford, England.

Tsai, J.S., Liao, C.L., 1999. Finite-element modeling of static surface errors in the peripheral milling of thin-walled workpieces. *Journal of Materials Processing Technology*, **94**(2-3):235-246. [doi:10.1016/S0924-0136(99)00109-0]

Wan, M., Zhang, W.H., Qiu, K.P., Gao, T., Yang, Y.H., 2005. Numerical prediction of static form errors in peripheral milling of thin-walled workpieces with irregular meshes. *Journal of Manufacturing Science and Engineering*, **127**(1):13-22. [doi:10.1115/1.1828055]

Wang, S.P., Padmanaban, S., 2004. A New Approach for FEM Simulation of NC Machining Processes. Proceedings of the 8th International Conference on Numerical Methods in Industrial Forming Processes, Columbus, Ohio, p.1371-1376.

Wang, Z.J., Chen, W.Y., Zhang, Y.D., 2005. Study on the machining distortion of thin-walled part caused by redistribution of residual stress. *Chinese Journal of Aeronautics*, **18**(2):175-179 (in Chinese).